Journal of Power Sources 269 (2014) 370–378

Contents lists available at ScienceDirect

Journal of Power Sources

journal homepage: www.elsevier.com/locate/jpowsour

Performance and stability of Pd nanostructures in an alkaline direct ethanol fuel cell

R. Carrera-Cerritos [a, b, c], R. Fuentes-Ramírez [c], F.M. Cuevas-Muñiz [a], J. Ledesma-García [b, **], L.G. Arriaga [a, *]

[a] Centro de Investigación y Desarrollo Tecnológico en Electroquímica, Parque Tecnológico Querétaro s/n, Sanfandila, Pedro Escobedo, Qro. C.P. 76703, Mexico
[b] Facultad de Ingeniería, División de Investigación y Posgrado, Universidad Autónoma de Querétaro, Centro Universitario Cerro de las Campanas, Querétaro, Qro. C.P. 76010, Mexico
[c] Departamento de Ingeniería Química, Universidad de Guanajuato, División de Ciencias Naturales y Exactas, Noria Alta s/n, Col. Noria Alta, Guanajuato, Gto. C.P. 36050, Mexico

HIGHLIGHTS

- Pd-nanostructures supported on C were evaluated as anode in an alkaline DEFC.
- Temperature effect and ethanol concentration on the power density were tested.
- Stability test was performed by applying 3 current density steps for 50 cycles.
- Strong morphological changes in the Pd-nanostructures were observed after test.
- Oxidative etching and Ostwald ripening were used to test morphology changes.

ARTICLE INFO

Article history:
Received 21 April 2014
Received in revised form
20 June 2014
Accepted 30 June 2014
Available online 7 July 2014

Keywords:
Direct ethanol fuel cell
Pd-nanopolyhedral
Pd-nanobar
Pd-nanorod

ABSTRACT

Pd nanopolyhedral, nanobar and nanorod particles were synthesised using the polyol process and evaluated as anodes in a direct ethanol fuel cell. The materials were physico-chemically characterised by high-resolution transmission electronic microscopy (HR-TEM), X-ray diffraction (XRD) and X-ray photoelectron spectroscopy (XPS). The effect of the operation parameters (i.e., temperature and fuel ethanol concentration) on the maximum power density (MPD) and open circuit voltage (OCV) was investigated. In addition, a stability test was performed by applying three current density steps for fifty cycles. The OCV values increased as the temperature increased for all of the catalysts at low ethanol concentration. Although the MPD increased with temperature for all of the catalyst independent of the ethanol concentration, the effect of the temperature on the MPD for each Pd structure results in different slopes due to the different crystal faces. Finally, a loss of electro-catalytic activity after fifty cycles was observed in all of the catalysts evaluated, which may be in response to morphological changes in the nanostructures.

1. Introduction

Direct ethanol fuel cells (DEFCs) have attracted considerable interest as promising carbon-neutral and sustainable power sources for portable, mobile, and stationary applications. Ethanol has a high energy density (8.0 kW h^{-1} kg^{-1}) and can be produced in great quantity from biomass via a fermentation process from renewable resources, such as sugar cane, wheat, corn, or straw [1]. DEFCs that use an anion membrane in alkaline media have several important advantages over conventional acid direct ethanol fuel cells. Examples of the advantages include (i) the possibility to use less expensive materials, such as Pd, Ni or Ag, than the typical Pt employed in acid media, (ii) enhancement of reaction kinetics at the cathode and anode, (iii) reduced alcohol crossover, and (iv) potential reduction of corrosion [2]. Despite these advantages, the design of highly active catalysts for the anode remains a challenge because the structure-sensitive ethanol electro-oxidation reaction (EOR) is difficult to induce and occurs at a slower rate.

The common strategies adopted to increase the activity of Pd (the most active metal for EOR in alkaline solutions) for EOR in alkaline media consist of alloying two or more metals as well as

* Corresponding author.
** Corresponding author.
E-mail address: larriaga@cideteq.mx (L.G. Arriaga).

http://dx.doi.org/10.1016/j.jpowsour.2014.06.161
0378-7753/

tuning the size and support type of the catalysts [3–5]. Recently, it has been shown that different crystallographic facets can be stabilised on particles with different shapes, and different activities and selectivities can be obtained with different facets. For example, polygonal Pd catalysts with dominant (111) facets exhibit excellent thermal stability and catalytic activity for formic acid electro-oxidation compared to the common Pd/C catalyst [6]. In addition, Pd and Pt nanocubes enclosed by (100) faces have exhibited extremely high activity for the oxygen reduction reaction and EOR in acidic media, respectively [7,8]. In addition, upon changing the morphology of the Pd catalysts from nanoparticles to nanorods with preferential (110) facets using electro-deposition, the specific activity increases 10-fold and becomes comparable to that of Pt under the operating potentials in H_2/O_2 fuel cells [9]. For EOR in alkaline solutions, enhanced activity for Pd nanowires, raspberry hollow Pd-nanospheres, and Pd-nanobars has been reported [10–12].

In recent years, the adsorption behaviour and oxidation mechanisms of ethanol over Pd surfaces including (111), (100) and (110) have been studied using density functional theory (DFT). The novel results indicated that the activity and selectivity of ethanol oxidation on Pd are highly structure-sensitive and confirmed that Pd (100) is the best surface for the dissociation of an ethanol molecule with a rather low energy barrier [13]. These observations were further supported by half-cell experiments [10].

Despite the excellent activity reported for Pd-nanostructures, a few studies have reported the performance of Pd or Pd-based materials with controlled morphology in a fuel cell environment. In addition, the stability test of these materials has been limited to half-cell experiments by chrono-amperometry. Therefore, three Pd-pure nanostructures named nanorod (NR), nanobar (NB), and nanopolyhedral (NP) nanoparticles were synthesised using the polyol process and supported on Vulcan carbon (C). The catalysts were physicochemically characterised by transmission electron microscopy (TEM), high resolution transmission electron microscopy (HRTEM), X-ray diffraction (XRD) and X-ray photospectroscopy (XPS). These catalysts were further evaluated as anodes in an anion-membrane DEFC in an alkaline medium. The effect of the ethanol concentration, cell temperature, and stability were also evaluated.

2. Experimental

2.1. Synthesis of the catalysts

The Pd-based catalysts were synthesised using a modified method for obtaining pure Pd nanostructures [14,12]. For NB/C, 10 cm^3 of ethylene glycol (EG, J.T. Baker, Austin, TX, USA, 99.9%) were placed in a 25 cm^3 three-neck flask equipped with a reflux condenser and a PTFE-coated magnetic stir bar. The flask was heated with an oil bath and stirred under static air at a constant temperature of 378 K. Meanwhile, 0.097 g of Na_2PdCl_4 (Sigma–Aldrich, St. Louis, MO, USA, 98%) and 1.2 g of KBr (J.T. Baker, Austin, TX, USA, 99%) were dissolved in 6 cm^3 of deionised water, and 0.183 g of polyvinylpyrrolidone (PVP, Aldrich, St. Louis, MO, USA, Mw = 55,000) were dissolved in 6 cm^3 of EG at room temperature (298 K). Then, the two solutions were simultaneously injected into the three-neck flask using two syringe pumps (Cole Palmer Instruments Company, Vernon Hills, IL, USA) at a rate of 90 $cm^3\ h^{-1}$. The reaction mixture was heated at 378 K while Vulcan carbon (0.05 g), which was previously heat treated at 550 K for 3 h, was added during the reduction process. After 1 h, the reaction was cooled to room temperature, and the product was separated by addition of 30 cm^3 of ketone and centrifuged at 4000 rpm for 20 min. The catalyst was dispersed in deionised water and separated by ultracentrifugation at 35,000 rpm for 2 h. The last process was repeated several times to remove the remaining impurities. Finally, the product was dried at 333 K for 12 h. A similar process was employed to produce the NP/C catalysts, except that the KBr was not added to the Pd precursor solution. The synthesis of the NR/C catalyst was analogous to that used to produce NB/C. However, the reaction temperature was maintained at 388 K in the NR/C synthesis.

2.2. Material characterisation

The crystalline nature of the catalysts was investigated using a Bruker D8 Advance X-ray diffractometer using Cu-Kα radiation operating at 40 kV and 40 mA over a 2θ range of 30–90° with a step size of 0.05° and a step time of 1 s. The diffraction patterns were compared to the Joint Committee on Powder Diffraction Standards (JCPDS). The specimens were prepared by ultrasonic dispersion in isopropyl alcohol, and a drop of the suspension was deposited on a carbon-coated grid prior to the TEM measurements. HRTEM and TEM analyses were conducted on a Titan 80-300 FEI apparatus operated at 300 kV to observe the detailed morphology and further calculate the fast Fourier transform (FFT) to obtain the electron diffraction pattern. The XPS characterisations were performed with a Versaprobe PHI 5000 system using Al monochromatic X-rays at 25 W and 15 kV. The survey and detailed spectra were obtained from 1 to 1000 eV and 331–345 eV with a step size of 0.5 eV and 0.05 eV and pass energy of 117.4 and 23.5 eV, respectively. The C 1 s peak was used as a standard for shifting corrections.

2.3. DEFC testing system

All of the fuel cell experiments were performed with a power station PSCOMPUCELL coupled to a DMFC (EC-DM) module (ElectroChem, Inc.). The test station controlled the rate, temperature, pressure and humidity of the air (Praxair, Mex., 19.5–23.5% O_2 + 76.5–80.5% N_2) flowing to the cathode as well as the cell operating temperature. Ethanol was pumped to the anode side of the fuel cell using a peristaltic pump internally coupled to the fuel reservoir. LabVIEW 5.1.1 software was used in the data acquisition system to control and measure the parameters of the fuel cell. Electrochemical impedance spectroscopy (EIS) was used to ensure reliability of the system before starting the polarisation measurements. The fuel cell testing system was coupled with a potentiostat/galvanostat Autolab POGSTAT 302 controlled by FRA software (EIS was recorded from 0.1 Hz to 10 kHz with amplitude of 10 mV). The 5 cm^2 fuel cell was used in all of the experiments. The fuel cell consisted of two stainless steel end plates and two graphite plates machined with serpentine flow fields. Two Teflon® gaskets were employed to ensure uniform MEA/GDL (Gas-diffusion layer) compression and to prevent damage to the MEA. An A201 membrane (Tokuyma, Japan) was used as an electrolyte after activation by immersion in 1 M KOH solution for 24 h followed by washing with deionised water. HT-ELAT (E-TEK) was used as the gas diffusion layer (GDL) at the anode and cathode. The GDL was painted with a catalytic ink composed of catalyst (67%) and Nafion® (33%). The membrane and electrodes were joined in the fuel cell plates, and the screws were tightened at 20 $lbin^{-2}$. Prior to the polarisation measurements, membrane rehydration and catalyst activation were performed. The membrane was rehydrated by feeding the anode with 7 ml min^{-1} of bi-distillate water for 15 min at room temperature. The catalyst was activated by running a few polarisation curves while 7 ml min^{-1} of 1 M ethanol was fed to the anode until reproducible curves were obtained. Intermediate air flow rate of 100 $cm^3\ min^{-1}$ was chose for all the experiments in order to avoid cathode flooding reported in A201 membranes, due the fact that diffusion flux from the anode to the cathode outweighs the

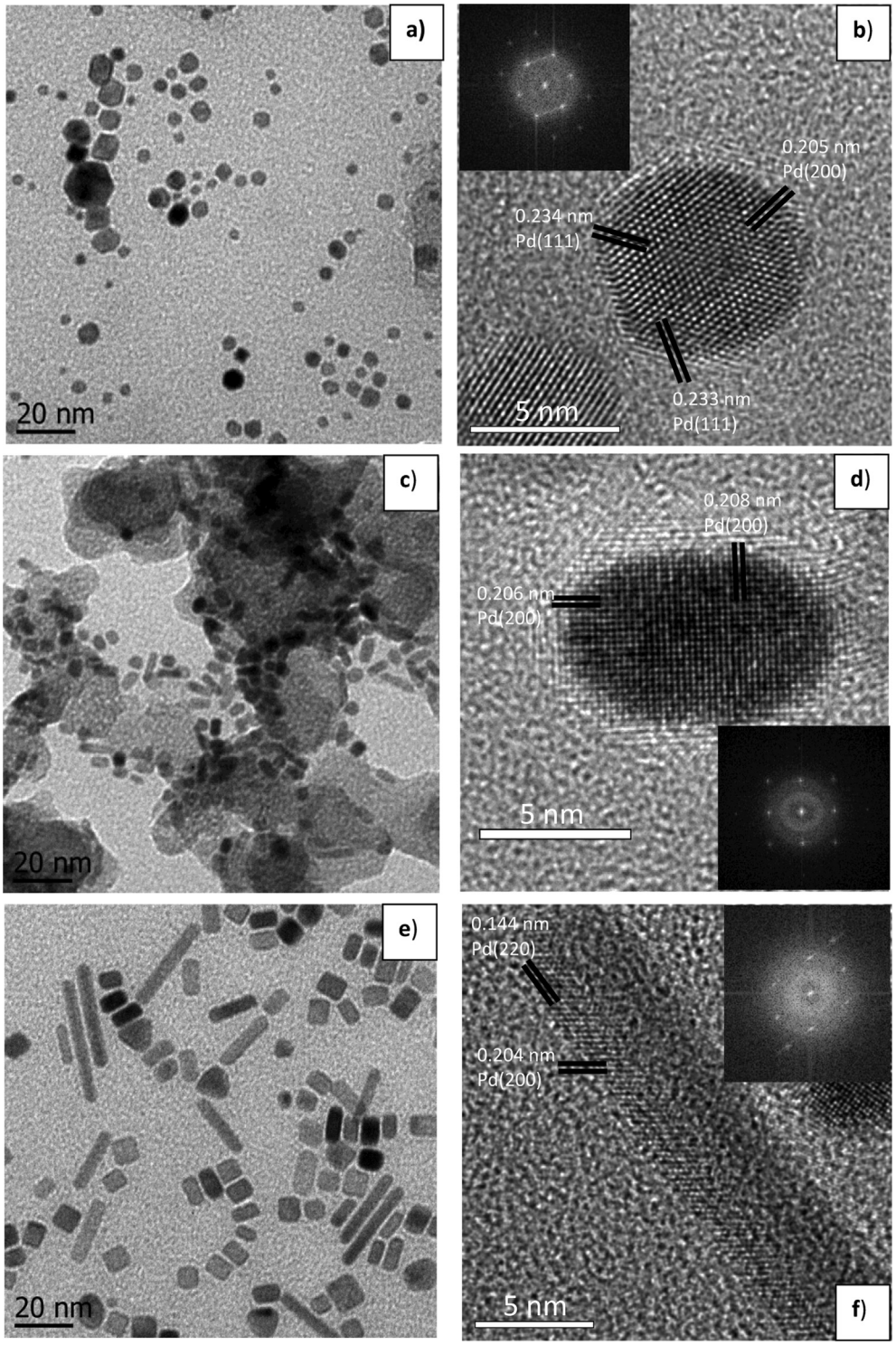

Fig. 1. TEM and HRTEM images for a)-b) NP/C, c)-d) NB/C, and e)-f) NR/C catalysts. Inset shows the FFT obtained from the respective HRTEM image.

total water flux due to the both ORR and electro-osmotic drag at low gas rates. However, this air flow rate would also allow water flux (originated by ethanol oxidation or coming from the ethanol solution) enough from the anode to the cathode for the ORR reaction [15–17]. Once reproducibility was obtained, the polarisation curves were constructed in the galvanostatic mode by imposing an electric current and recording the potential measurement after stabilisation for 2 min. The stability test consisted of 50 cycles of three current density steps. After cycling, the other polarisation curves were recorded and compared to the curves measured prior to cycling.

3. Results and discussion

3.1. TEM and HRTEM

The TEM experiments were performed to observe the shape, size and dispersion of the synthesised Pd-nanostructures over the

support (Fig. 1). Fig. 1a and b indicate that the NP/C catalyst is composed of polyhedral nanoparticles with an average diameter of 5.3 nm. These polyhedral nanoparticles preferentially expose Pd (111) faces, and Pd (200) fringes were also observed. As shown in Fig. 1c and d, most of the nanoparticles on the carbon support consisted of Pd nanobars with a particle size of approximately 4 nm (width) × 4–10 nm (length). In addition, the *d* spacing of the Pd nanobars was 2.06–2.08 nm, which corresponds to the (200) fringes of Pd with a face centred cubic structure. The well-defined fringes in the nanobar indicate that it is monocrystalline and surrounded by (100) facets. In contrast to the nanobar-based catalysts, the NR/C catalyst exhibits a mixture of nanobars and nanorods. The size of the nanorods was 5 nm (width) × 15–80 nm (length). The nanobars are larger (5–7 nm (width) × 5–12 nm (length)) than those observed in the NB/C catalysts (Fig. 1e). HRTEM images indicate fringes that were not well resolved due the limited resolution of the equipment. However, the electron diffraction (ED) obtained by FFT indicates the presence of (110) and (100) planes. This observation was possible due to the nanorods possessing an octagonal crossed-section with its side bounded by a mixture of alternating (100) and (110) faces. The absence of cubic symmetry in the FTT (inset in Fig. 1f) indicates that this nanorod was supported on the TEM grid against the face (110). In addition, the ED shows the (111) plane. The presence of the (111) face on the sides of the Pd nanorods has also been previously observed and is associated with surface reconstruction caused by the transformation of (110) into strips of (111) faces [14].

3.2. XRD analysis

The XRD patterns of the palladium-based nanostructures are shown in Fig. 2. In general, the patterns of the Pd catalysts indicate a crystalline structure with peaks located at 40.119°, 46.659°, 68.121°, 82.1° and 86.619°, which correspond to the (111), (200), (220) and (311) fringes of the face centred cubic structure (*fcc*) of Pd (JCPDS 46–1043). The diffraction peaks at approximately $2\theta = 25°$ for all of the catalysts were assigned to the reflections of the carbon support. The average crystal size was calculated based on broadening of the (111), (200) and (220) diffraction peaks according to the Scherrer equation, as shown in Table 1. These sizes are in good agreement with the previous values determined from the TEM images (smaller side of each nanostructure). In addition, the Pd (111)/Pd (200) ratio was estimated to be 2.05 for NB/C. This ratio is lower than the theoretical value of 2.38, which was reported for polycrystalline Pd with a typical *fcc* structure [18]. This result confirmed the preferential exposure of the (100) surface of the nanobar-based catalyst. However, a ratio of 2.5 was obtained for the NP/C catalysts, which confirmed the preferential exposure of the (111) surfaces of the Pd-polyhedral structures observed by HRTEM, which is in agreement with previously reported results [18]. Therefore, the surface exposition of Pd-nanobars, nanorods and nanopolyedral nanoparticles (inferred by XRD and HRTEM in Sections 3.1 and 3.2) is consistent with results previously reported for similar Pd nanostructures synthesised by polyol process [6,14,19–24].

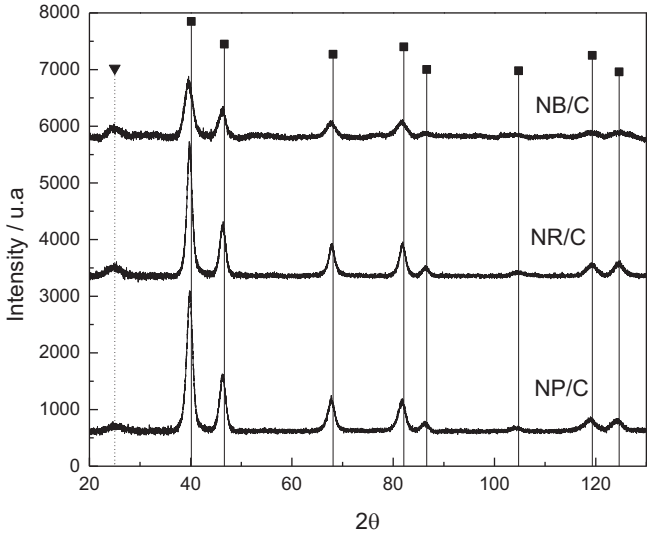

Fig. 2. XRD patterns recorded for all of the studied catalysts. (Filled triangles correspond to carbon reflections, and black squares indicate Pd with a *fcc* structure).

3.3. XPS characterisation

The surface composition of the nanoparticles was determined by XPS and is shown in Fig. 1. In addition to C and Pd, the survey scan (not shown) indicated the presence of impurities, such as oxygen and bromide residuals on the catalyst surface. A further detailed scan in the specific regions was used to calculate these impurities and analyse the oxidation states of Pd in the catalysts. A combined O and Br content of 8.9, 12.0 and 13.5% wt. was determined for NP/C, NB/C and NR/C, respectively. The high content of oxygen and bromide suggests the presence of a film of Pd oxides that commonly coexist at the surface of palladium nanoparticles exposed to the air but thin enough to avoid being detected by XRD [20].

Fig. 3 shows the detailed XPS spectra recorded in the Pd $3d_{5/2}$ region. Different oxidation states of Pd can be appreciated after deconvolution of all of the catalysts. 76.8, 67 and 52% metallic Pd^0 (peak I) were determined for NP/C, NR/C and NB/C, respectively. The remaining Pd in the Pd-pure catalysts consisted of Pd^{2+} species (peak II). The Pd 3*d* binding energy for Pd^0 and Pd^{2+} is in agreement with the position of binding energies previously reported for Pd/C nanoparticles [19]. The high content of Pd^0 in the NP/C catalysts is due to the absence of Br^- ions that form the more stable $PdBr_4^{2-}$, respectively. However, the low Pd^0 concentration on the surface of NB/C and NR/C were due to the slow reduction rate of Pd required to achieve unidirectional growth.

3.4. Fuel cell performance

3.4.1. Temperature and ethanol concentration effects on the OCV

The fuel cell experiments were performed using different ethanol concentrations and temperatures. Table 2 lists the open circuit potentials (OCV) measured in each experiment, which are in agreement with other OCVs reported in the literature and are very close to the theoretical value in a DEFC operating under alkaline conditions (1.14 V). This result indicates high catalytic activity at the electrodes [21]. Song et al. reported that the OCV was substantially affected by temperature due to a direct and enhancing effect of the reaction kinetics at the anode [19–22]. However, the temperature effect with a 3 M ethanol solution was the opposite of that in a 1 M ethanol solution because the OCV slightly decreased as the temperature increased for all of the catalysts. In this case, the fuel

Table 1
Structural parameters obtained from the XRD patterns for the synthesised catalysts.

	a (XRD)/Å	Crystal size/nm	(111)/(200)	(111)/(220)
NP/C	3.90	6.3	2.50	4.68
NR/C	3.91	6.7	2.43	4.38
NB/C	3.91	5.1	2.05	4.06

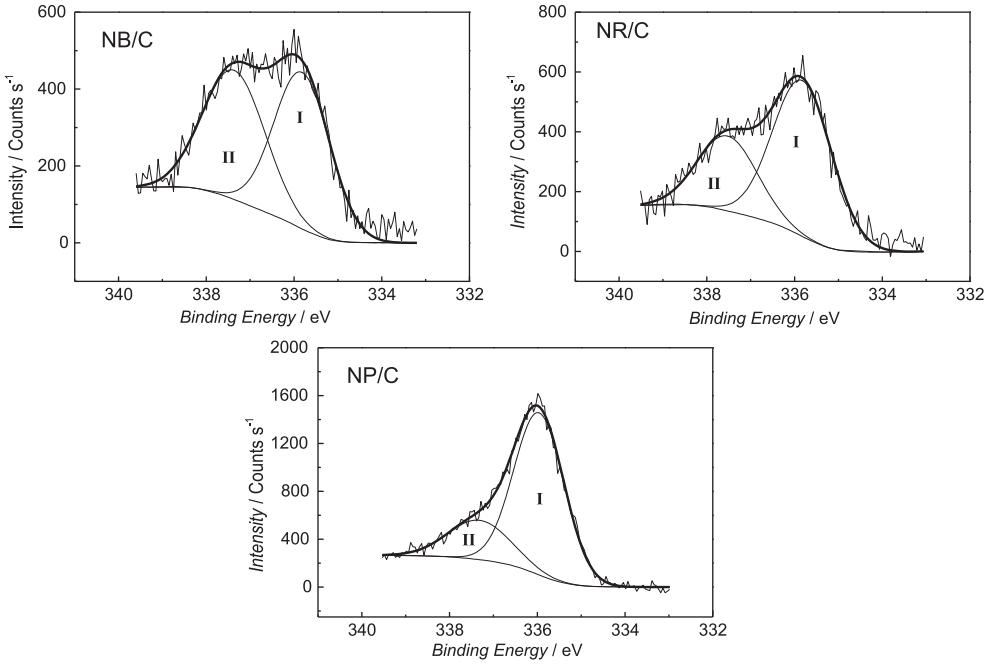

Fig. 3. XPS spectra obtained for the Pd-based nanostructured catalysts.

crossover is a thermally activated process. When the temperature increases, the polymeric membrane expands allowing for higher transport rates. In addition, the ethanol diffusivity is enhanced. These two phenomena were highly promoted by the higher ethanol concentration difference between the cathode and anode with 3 M ethanol compared to 1 M ethanol, which resulted in high ethanol permeation to the cathode causing a decrease in the cathode activity.

3.4.2. Temperature and ethanol concentration effects on fuel cell performance

For the fuel cell performance, Fig. 4 shows the polarisation behaviour of the catalysts with 3 M ethanol. All of the results for the maximum power density (MPD) are summarised in Fig. 5. Density functional theory studies confirmed that Pd (100) is the best surface for the dissociation of an ethanol molecule due to the strong ethanol-Pd (100) interaction, which leads to the lowest energy barrier relative to those of the Pd (111) and Pd (110) surfaces [13]. This theoretical observation was observed in half cell experiments, and the results indicated that the Pd nanobars enclosed by (100) surfaces exhibited the highest activity followed by the polyhedral nanoparticles with preferential (111) surfaces and nanorods surrounded by a mixture of the three low-index surfaces [10]. In the current study, the same MPD sequence was observed using 3 M ethanol and 298 K where the MPD values were 8.1, 6.8 and 6 mW cm^{-2} for NB/C, NP/C and NR/C, respectively. The MPD increased as the temperature increased for all of the catalysts in both the 1 M and 3 M ethanol solutions due to the faster electrochemical kinetics, increased conductivity of OH^- ions, and enhanced mass transfer [23]. Therefore, this order did not remain at 323 and 343 K, which suggested differences in the enhanced activity with temperature over the catalysts associated with the kinetic dissimilarities due to the different crystal faces. For example, the NP/C catalysts exhibited a smaller enhancing effect with temperature in the 1 and 3 M ethanol solutions because the MPD slightly increased when the temperature changed from 298 to 323 K. However, the MPD at 343 K remained unchanged and was slightly higher for the 3 M and 1 M ethanol solutions, respectively.

Table 2
Open circuit voltages measured for all of the catalysts at 298, 323 and 343 K in 1 and 3 M ethanol solutions.

	OCV/V			
	T/K	NP/C	NR/C	NB/C
1 M	298	0.96	0.98	0.86
	323	1	1	0.91
	343	1.05	1	0.93
3 M	298	0.95	0.9	0.86
	323	0.92	0.9	0.85
	343	0.93	0.91	0.85

It has been previously suggested that the rate-limiting step of ethanol electro-oxidation involves the reaction of ethoxy species with OH^- via Equation (1).

$$Pd\text{-}(CH_3CO)_{ads} + Pd\text{-}OH_{ads} \rightarrow Pd{-}CH_3COOH + Pd \quad (1)$$

The surface area covered by ethoxy species can gradually increase as the ethanol concentration increases leading to a greater amount of ethoxy species on the Pd surface. However, the adsorption of hydroxyl groups is largely blocked by CH_3CO species. As indicated by Equation (1), the insufficient coverage of OH^- ions with 3 M ethanol will lead to a decrease in the peak current, which is only achieved with an intermediate coverage of the ethoxy and hydroxyl adsorbates [10].

It should be noted in Fig. 4, that the current densities were low in the this work compared to mathematical models and experimental results reported for direct ethanol fuel cells (DEFC) employing a patented catalyst and optimum operation conditions due to the use of oxygen at a high pressure and fuel cell hardware with a low resistance ($\approx$MPD 60 mW cm^2 and maximum current density of $\approx$500 mA cm^{-2}) [24]. In addition to the use of air as an oxidant at atmospheric pressure and the preparation of the MEAs with no hot-pressing step, the use of Nafion as a catalyst binder without suitable ionic conduction at 1 M KOH could result in low current densities due to the increase of the internal resistance [25].

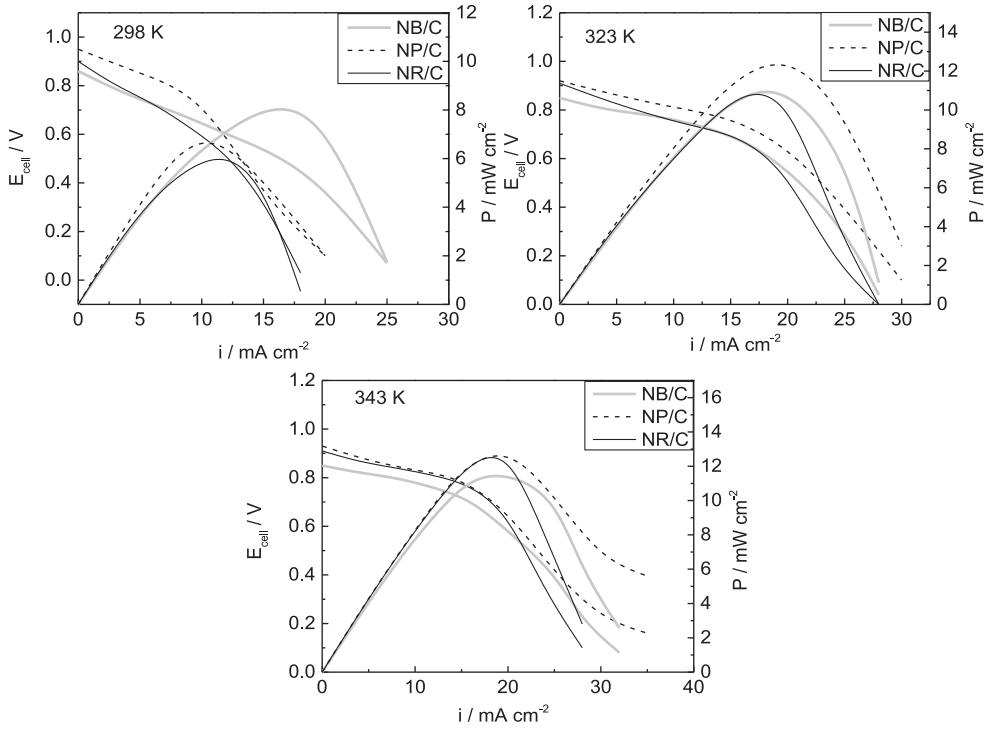

Fig. 4. Effect of the Pd nanostructures on the fuel cell performance at different temperatures. Conditions: Air at atmospheric pressure and 100 cm^3 min^{-1}, 3 M ethanol, 7 cm^3 min^{-1} flow rate.

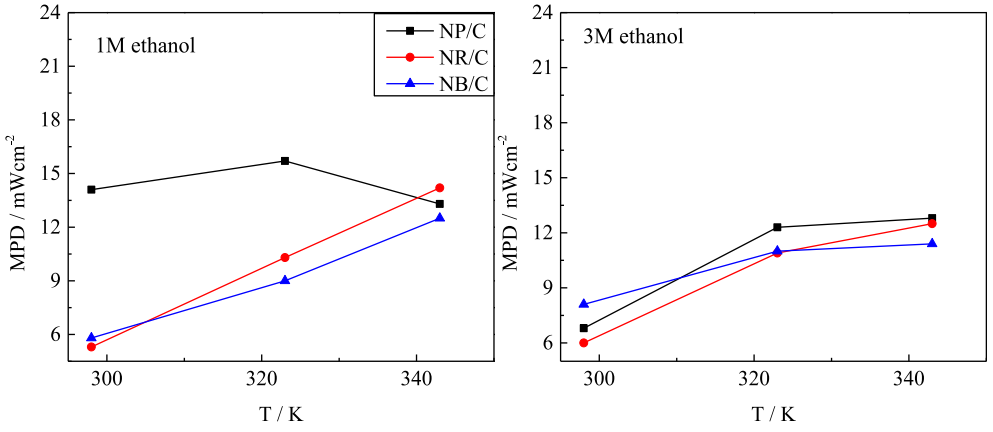

Fig. 5. Effect of the temperature on the MPD for the Pd-based nanocatalysts with 1 M and 3 M ethanol solutions. Conditions: Air at atmospheric pressure and 100 cm^3 min^{-1}, anode flow rate: 7 cm^3 min^{-1}.

On the other hand, provided that the thin layer of surface Pd oxides [25] can be reducible during the conditioning step by the polarizations curves, the oxygen contribution should not be quantified as impurities. Therefore, the remaining impurities provided in XPS section would be 0, 4.4 and 6.6% wt. for the NP/C, NB/C and NR/C catalysts, respectively. Considering these low percentages, it was assumed that they did not affect significantly the decrease in polarization curves.

3.4.3. Stability fuel cell performance

According to previous studies, metal nanostructures exhibited excellent electrochemical activity for the oxidation of small organic molecules and the oxygen reduction reaction in half cell experiments. For example, Lee et al. reported that (111) surfaces in polygonal-Pd/C catalysts exhibited good thermal stability and excellent catalytic activity for formic acid electro-oxidation. In addition, Pd (alkaline) and Pt (acid) nanocubes with (100) facets exhibited good activity in terms of the low onset potential and/or high current density for the ethanol electro-oxidation reaction. However, there are very few reports on the stability of these nanostructures under the fuel cell environment. To study the stability of the Pd nanostructures as the anode in the current work, the fuel cell was operated at three different current values and cycled 50 times (Inset in Fig. 6, NP/C shown as example). Fig. 6 shows the polarisation curves obtained before and after the cycling process. First, the OCV slightly increased after the cycling process for all of the catalysts, which indicated that thermodynamic electrochemical properties of the ethanol electro-oxidation and oxygen reduction reactions were not affected during the study.

For the NB/C and NP/C catalysts, the maximum current density was nearly constant before and after the stability test. However, their MPD was approximately 1 mW cm^{-2} lower than at the

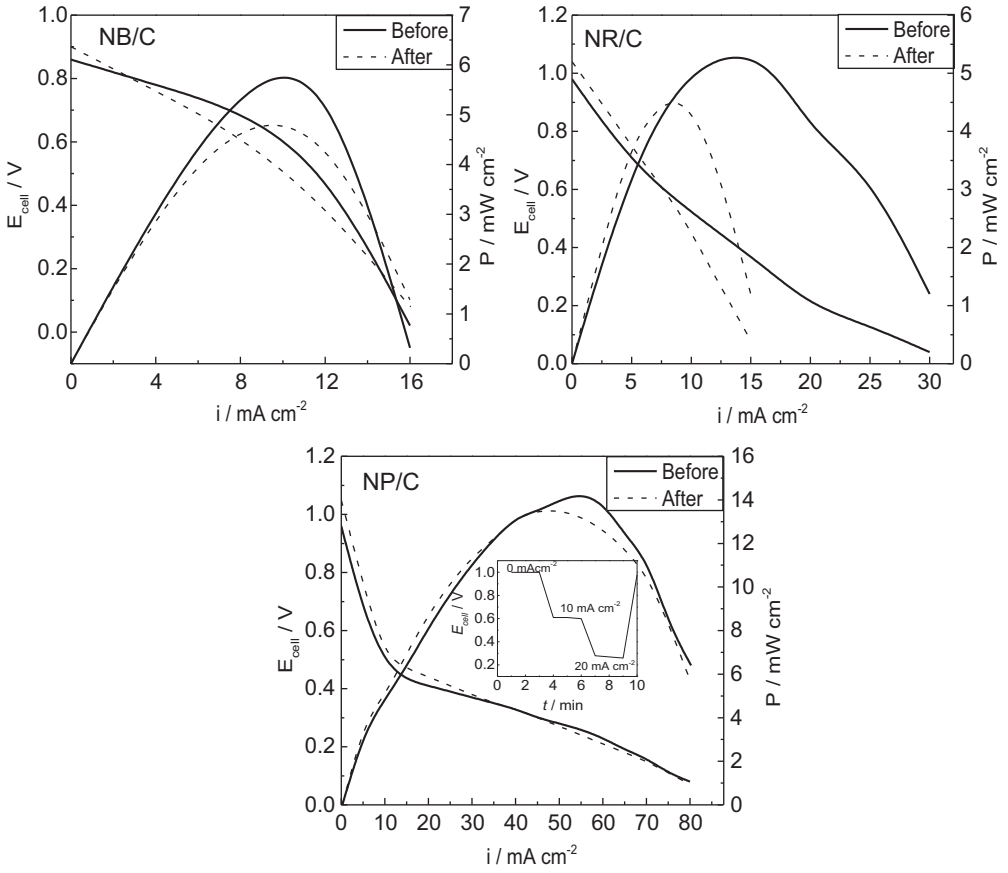

Fig. 6. Polarisation curves obtained before and after 50 cycles of 3 current density steps (inset figure, NP/C). Conditions: Air at atmospheric pressure and 100 cm^3 min^{-1}, $T = 298$ K, 1 M ethanol/1 M KOH solution and 7 cm^3 min^{-1}.

beginning. The NR/C catalyst exhibited the lowest stability with a decrease of 15 mA cm^{-2} in the maximum current density.

TEM studies of the Pd-based nanostructures were performed after the stability analysis (Fig. 7). Various degrees of morphological modification were observed in all of the catalysts. For the NB/C catalyst, a few nanobars with a size of 3.8–4.2 (width) × 7–9 nm (length) were observed. Most of the original nanobars evolved to irregular nanoparticles with an average diameter of 5.8 nm. According to thermodynamics, the free surface energy of a nanocrystal composed of a face centred cubic metal, which also corresponds to the surface activities, increased in the following order: $\gamma(111) < \gamma(100) < \gamma(110)$. Therefore, minimisation of the surface energy of a particle was the main driving force for the evolution from Pd nanobars with preferential (100) faces to nanoparticles with a mixture of (111) and (100) planes [14]. Recently, it was reported that Pd nanocubes can only be transformed into cuboctahedral nanocrystals in the presence of air. The presence of oxygen in the reactive solution allows for surface oxidative etching leading to complete surface modification [26]. Therefore, in parallel to the thermodynamic instability of Pd-nanobars, the presence of oxygen in the ethanol solutions may be another cause for the decrease in the fuel cell performance. This observation could partially explain the discrepancy in the performance of the Pd nanostructures for the ethanol electro-oxidation reaction in half cell experiments that was previously reported [10] and in the fuel cell results obtained in this study because the air is always removed in the half cell experiments, which prolongs the stability of the Pd nanostructures.

The NP/C catalyst exhibited a low morphological and size modification in the current study where the average size slightly increased from 5.3 to 8.4 nm (Figs. 1 and 7, respectively). The increase in the particle size may be due to the Ostwald ripening process where surface atoms detach from the smaller nanoparticles followed by reattachment of these atoms to the more stable surfaces of the larger nanoparticles [27]. The nanobar and nanopolyhedral–based catalysts exhibited a smaller fuel cell performance loss after the stability test, which may be due to a smaller morphology modification in these catalysts. In contrast, the NR/C catalysts exhibited a large shape modification because only larger nanorods were observed after the cycles, and the occurrence of irregular Pd nanoparticles with an average size of 15.2 nm were observed. This strong surface modification was in agreement with the order of surface energy mentioned above because the nanorods exposed high-energy surfaces (i.e., (100) and (110)) on the sides. In addition, the removal of the capping ligands has also been reported as a source of surface modification in gold nanorods [28].

The decrease in the current density observed for the NR/C catalysts after fuel cell evaluation may be due to deep modification of the morphology, which decreased the prevalence of the (200) fringes, and growth of the nanoparticle size under the reaction conditions, which resulted in a reduction of active sites.

4. Conclusions

The performance and stability of Pd nanopolyhedral particles, nanobars and nanorods synthesised with the polyol process for use as an anode in a direct ethanol fuel cell were investigated. The materials were physicochemically characterised by TEM-HRTEM, XRD and XPS. The effect of the temperature and ethanol concentration on the OCV and MPD were evaluated, and the stability was

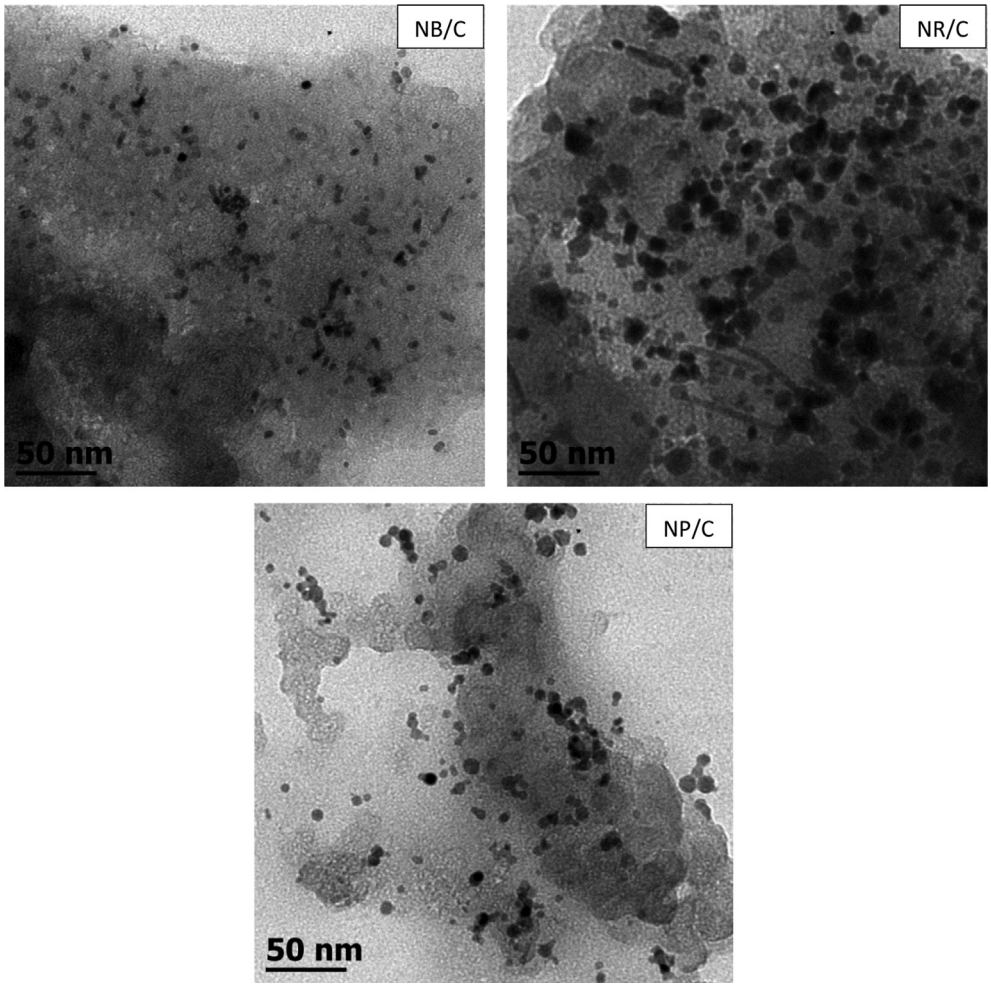

Fig. 7. TEM images of the catalysts after the fuel cell experiments and cycling process.

tested by applying three current density steps for fifty cycles. The OCV values increased as the temperature increased for all of the catalysts analysed in 1 M ethanol. However, the OCV decreased with the temperature in 3 M ethanol, which was due to higher fuel crossover. Although the MPD increased with temperature in all of the catalyst in the 1 M and 3 M ethanol solutions, the effect of temperature on the MPD for each Pd structure exhibited a different slope due to the different crystal faces. A loss of electro-catalytic activity after fifty cycles was observed in all of the studied catalysts. The NB/C and NP/C catalysts exhibited a slight loss in MPD, with good fuel cell stability maintaining the MPD with only a slightly change after 50 cycles.

The changes in the Pd nanostructures after the fuel cell cycles were due to morphological modifications that occurred to a different extent in each catalyst. Various concepts were used to explain the morphology modification, including the thermodynamic stability of crystal faces, oxidative etching and Ostwald ripening.

Acknowledgements

The authors acknowledge the use of the WVU Shared Research Facilities (XPS data) and M.T. Carrillo (UG) for the document revision. Thanks to CONACYT for financial support through project Fomix-Querétaro grant 193148. R. Carrera-Cerritos wish to thank CONACYT for the financial support during his Ph.D. studies, Grant No. 213850.

References

[1] T.S. Zhao, Y.S. Li, S.Y. Shen, Front. Energy Power Eng. China 4-4 (2010) 443–458.
[2] E. Antolini, E.R. Gonzalez, J. Power Sources 195 (2010) 3431–3450.
[3] S.Y. Shen, T.S. Zhao, J.B. Xu, Electrochim. Acta 55 (2010) 9179–9184.
[4] E.H. Yu, U. Krewer, K. Scott, Energies 3 (2010) 1499–1528.
[5] H.T. Zheng, Y. Li, S. Chena, P.K. Shen, J. Power Sources 163 (2006) 371–375.
[6] Y.W. Lee, J.K. Oh, H.S. Kim, J.K. Lee, S.B. Han, W. Choi, K.W. Park, J. Power Sources 195 (2010) 5896–5901.
[7] S.B. Han, Y.J. Song, J.M. Lee, J.Y. Kim, K.W. Park, Electrochem. Commun. 10 (2008) 1044–1047.
[8] S. Xie, S.-I.I. Choi, X. Xia, Y. Xia, Curr. Opin. Chem. Eng. 2 (2013) 142–150.
[9] L. Xiao, L. Zhuang, Y. Liu, J.T. Lu, H.D. Abruña, J. Am. Chem. Soc. 2 (2009) 602–608.
[10] C. Xu, H. Wang, P. Shen, P. Jiang, Adv. Mater. 19 (2007) 4256–4259.
[11] Z. Liu, B. Zhao, C. Guo, Y. Sun, Y. Shi, H. Yang, Z. Li, J. Colloid Interface Sci. 351 (2010) 233–238.
[12] R. Carrera-Cerritos, M. Guerra-Balcázar, R. Fuentes-Ramírez, Janet Ledesma-García, L.G. Arriaga, Materials 5 (2012) 1686–1697.
[13] E.D. Wang, J.B. Xu, T.S. Zhao, J. Phys. Chem. C. 114 (2010) 10489–10497.
[14] Y. Xiong, H. Cai, B.J. Wiley, J. Wang, M.J. Kim, Y. Xia, J. Am. Chem. Soc. 129 (2007) 3665–3675.
[15] Y.S. Li, T.S. Zhao, J.B. Xu, S.Y. Shen, W.W. Yang, J. Power Sources 196 (2011) 1802–1807.
[16] M.Z.F. Kamarudin, S.K. Kamarudin, M.S. Masdar, W.R.W. Daud, Int. J. Hydrogen Energy 38 (2013) 9438–9453.
[17] Y.S. Li, T.S. Zhao, R. Chen, J. Power Sources 196 (2011) 133–139.
[18] Y. Chen, B. He, T. Huang, H. Liu, Colloids Surfaces A: Physicochem. Eng. Aspects 348 (2009) 145–150.

[19] Y. Xiong, H. Cai, Y. Yin, Y. Xia, Chem. Phys. Lett. 440 (2007) 273–278.
[20] C.M. Ghimbeu, C. Zlotea, R. Gadiou, F. Cuevas, E. Leroy, M. Latroche, C. Vix-Guterl, J. Mater. Chem. 21 (2011) 17765–17775.
[21] L. An, T.S. Zhao, R. Chen, Q.X. Wu, J. Power Sources 196 (2011) 6219–6222.
[22] S. Song, W. Zhou, J. Tian, R. Cai, G. Sun, Q. Xin, S. Kontou, P. Tsiakaras, J. Power Sources 145 (2005) 266–271.
[23] Y.S. Li, T.S. Zhao, Z.X. Liang, J. Power Sources 187 (2009) 387–392.
[24] L. An, Z.H. Chai, L. Zeng, P. Tan, T.S. Zhao, Int. J. Hydrogen Energy 38 (2013) 14067–14075.
[25] H. Hou, S. Wang, W. Jin, Q. Jiang, L. Sun, L. Jiang, G. Sun, Int. J. Hydrogen Energy 36 (2011) 5104–5109.
[26] W.U. Binghui, Zhang Huihui, Zheng Nanfeng, Mechanism of Cube-to-Cuboctahedron Morphology Transformation of Pd Nanocrystals[OL], 15 February 2012. http://www.paper.edu.cn/en_releasepaper/content/4463466.
[27] R. Narayanan, M.A. El-Sayed, J. Phys. Chem. B. 109 (2005) 12663–12676.
[28] Z.L. Wang, R.P. Gao, B. Nikoobakht, M.A, J. Phys. Chem. B. 104 (2000) 5417–5420.